Thermodynamic, transport and viscoelastic properties of PBX-9501 binder: A molecular dynamics simulations study

Hemali Davande, Dmitry Bedrov and Grant D. Smith*

Department of Materials Science and Engineering
122 South Central Campus Drive, Room 304, University of Utah, Utah, 84112

Abstract

Atomistic molecular dynamics simulations were performed on a low molecular weight nitroplasticized Estane® mixture representative of the binder used in PBX-9501. Pressure-volume-temperature (PVT) behavior over a wide range of pressure and temperatures above the order-disorder temperature (ODT) of Estane was determined and represented with the empirical Tait and Sun equations-of-state. The effect of temperature, pressure and plasticization on transport properties of the mixture was also examined. A combination of molecular dynamics simulations and theoretical reptation models was used to predict the shear stress relaxation modulus $G(t)$ of PBX-9501 binder at 473 K and 1 atm pressure. Data obtained from simulations of the model PBX-9501 binder presented here can be utilized to predict the temperature and pressure dependence of the shear stress relaxation modulus for temperatures above the ODT.

I. Introduction

Plastic bonded explosives (PBXs) typically consist of grains of an energetic material such as 1,3,5,7-tetranitro-1,3,5,7-tetraazacyclooctane or hexahydro-1,3,5-trinitro-1,3,5-triazine (HMX) held together by a polymer matrix, or binder. Typically, PBX-9501, which is an HMX-based explosive, comprises of about 95 wt% HMX and 5 wt% binder. The binder for PBX-9501 is a 1:1 mixture of Estane®, a polyester polyurethane block co-polymer, and a eutectic mixture of bis(2,2-dinitropropyl)formal (BDNPF) and bis(2,2-dinitropropyl)acetal (BDNPA). Hereafter this Estane/nitroplasticizer mixture will be referred as model PBX-9501 binder.

While comprising only about 5% of the composite by weight, the PBX-9501 binder has a dramatic influence on the properties and response of the explosive. The binder in PBXs imparts structural integrity to the composite, aids in its processing and decreases the sensitivity of explosive to the external stimuli [1,2]. Importantly, the properties of the binder are much more sensitive to temperature, pressure and thermal history than those of HMX. Hence, the softening of the binder at the elevated temperatures can dominate mechanical response of the composite. Increased sensitivity of thermally damaged PBX-9501 has been linked to thermally induced mesoscopic chemical and morphological changes in the explosive [2]. These changes in turn are assumed to be partly related to the decreased binder viscosity and the decomposition at elevated temperatures [3]. It has also been suggested that hot spots or regions of local heating within the explosives can be generated by mechanical deformation of the polymer binder phase [4,5]. While rubbery at atmospheric pressure, the shear modulus in PBXs binders can increase up to three orders of magnitude under pressure increases as low as 0.5 GPa [6]. It is known that under shock loading conditions (where pressures are of the order of GPa or greater), the polymer relaxation time increases dramatically [7,8].

II. Molecular Dynamics Simulations

In this work we have undertaken molecular dynamics (MD) simulations to investigate the thermodynamic and viscoelastic properties of a model PBX-9501 binder over a range of pressure and temperature. An ensemble of 14 copolymer chains of Estane, 56 molecules of BDNPF and 54 molecules of BDNPA was generated. Each copolymer chain of model Estane (MW= 2510Da) had the structure $S_2H_1S_5H_1S_2$, where 'S' represents a poly(butylene adipate) soft segment with one 1,4-butanediol (BDO) linkage and 'H' represents a bis-1,1'-(methyl phenyl-4-isocyanate) (diphenyl-methane diisocyanate) unit with one BDO linkage. The chemical structures of the soft and the hard segments of Estane are illustrated in Fig. 1(a). The binder system so formed was a 1:1 mixture by weight of Estane and nitroplasticizer. The chemical structures of nitroplasticizer used in model PBX-9501 binder are illustrated in Fig. 1(b). For simulations of model pure Estane, only the 14 copolymer chains were used. Previously developed quantum chemistry based force fields for Estane [9] and BDNPF/A nitroplasticizer [10] were used in the simulations. For nonbonded interaction between atom pairs not explicitly defined in the force fields, standard combining rules (geometric means for energy parameters, arithmetic means for distance parameters) were used to define exponential-6 type nonbonded functions.

All molecules were initially placed on a low-density cubic lattice with periodic boundary conditions at 700 K. The cubic system was simulated for about 3ns using NPT (constant number of particles, pressure and temperature) ensemble while the volume was decreased to yield an average pressure of 1 atm. Then, starting with the configuration so obtained, the temperature and pressure were gradually changed to cover the range of applied pressure (1 atm – 8000 atm) and temperature (298 K–700 K).

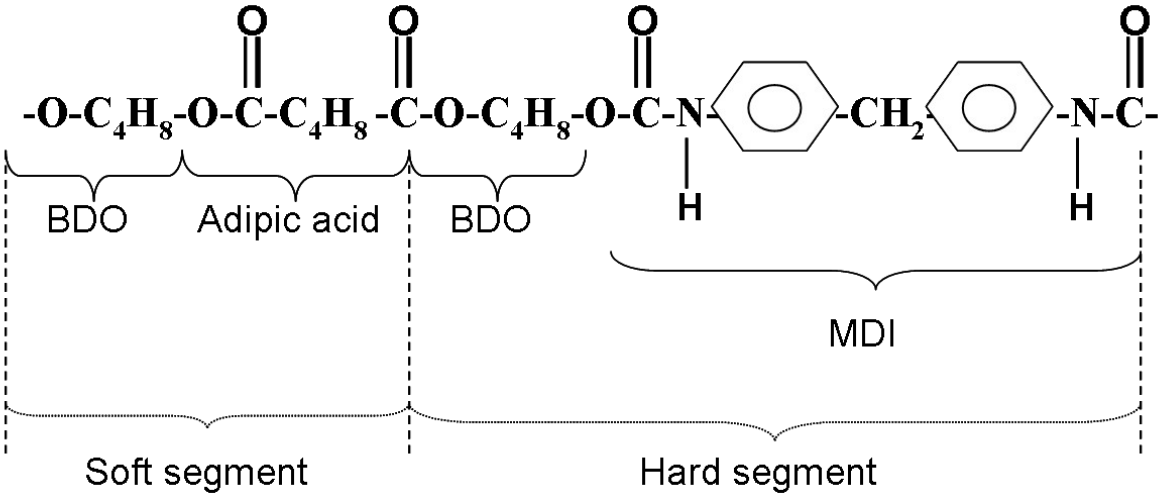

Figure 1(a)

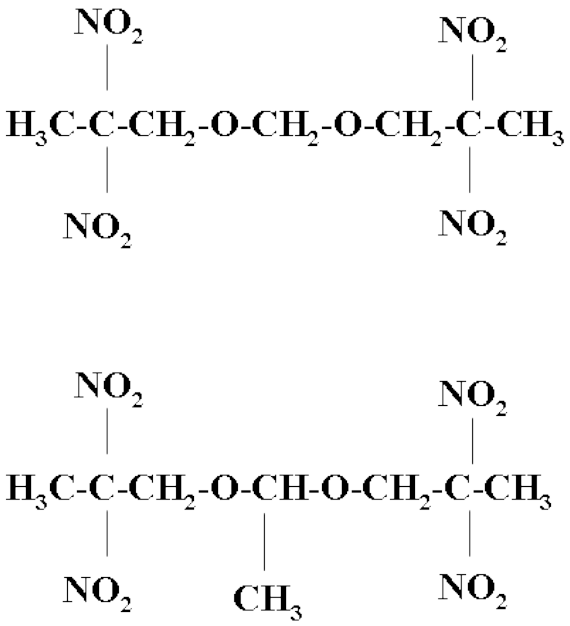

Figure 1(b)

Figure 1. Chemical structure of (a) repeat units in Estane and (b) bis(2,2-dinitropropyl)formal or BDNPF (top) and bis(2,2-dinitropropyl)acetal or BDNPA (bottom).

For each pressure and temperature studied, equilibration for about 10 ns was conducted in the NPT ensemble. Production runs over more than 10 ns were conducted in the NVT ensemble (details in Table 1).

Table 1

Details of simulation runs

System	Pressure/Temperature	Simulation time NPT (ns)	Simulation time NVT (ns)
		600 K and 700 K isotherms	
Binder	1 atm	10 (12)	43 (38)
	500 atm	12 (10)	18 (13)
600 K	1000 atm	10 (12)	18 (13)
	2000 atm	12 (7)	13 (13)
(700 K)	3000 atm	10 (9)	17 (12)
	4000 atm	12 (6)	12 (12)
	6000 atm	15 (9)	12 (11)
	8000 atm	12 (7)	12 (12)
		1 atm isobar	
Binder	298 K	20	51
	350 K	16	-
1 atm	473 K	25	61
	550 K	17	-
	600 K	10	43
	700 K	12	38
Estane	298 K	49	-
	473 K	10	92
1 atm	600 K	6	45
	700 K	6	25

The MD simulation package *Lucretius* [11] having the Nose-Hoover thermostat [12,13] and Anderson-Hoover barostat [25,14] was used for all simulations. Covalent bond lengths were constrained using the SHAKE algorithm [15]. A cut-off radius of 10Å was used for all van der Waals interactions. In order to account for long range electrostatic interactions, Particle Mesh Ewald (PME) algorithm [16] was used. The time step for the reciprocal part of PME calculations

was 2 fs. A multiple time step reversible reference system propagator algorithm described elsewhere [17] was employed for integrating equations of motion. The time step of integration for high frequency vibrations (bends and torsions) was 0.5 fs. Nonbonded interactions within a cut-off radius of 6 Å were evaluated every 1 fs, while those between 6 Å and 10 Å were evaluated every 2 fs. The atomic stress tensor (employed in shear viscosity and time-dependent shear stress relaxation modulus calculations described below) was recorded every 10 fs.

The longest relaxation time for the systems simulated, defined by the model Estane chain (2510 Da) end-to-end vector auto-correlation function in the pure melt at 473 K, was about 50 ns. It was not possible for us to carry out high pressure studies at 473 K and still achieve reliable transport properties. Hence in order to study the effect of pressure (1 atm - 8000 atm) isotherms at 600 K and 700 K were studied. To investigate the influence of temperature on binder dynamics the atmospheric isobar was investigated at 298 K, 350 K, 473 K, 550 K, 600 K and 700 K for the model PBX-9501 binder. To study the effect of plasticization, properties of pure Estane at 298 K, 473 K, 600 K and 700 K were also determined at 1 atm. A detailed summary of all simulation performed is given in Table 1.

III. Data analysis

NPT simulations were used to extract equilibrium volume (and hence the density), thermal expansion coefficients and bulk moduli. Using the equilibrated volume so obtained, production runs with constant number of particles, volume and temperature, or NVT ensemble, were carried out. The transport properties (diffusion coefficient and viscosity) and viscoelastic response of the binder were obtained from the NVT data.

A. Equations-of-state

The isothermal pressure-volume (PV) data from our MD simulations were fit with the empirical Tait [18] equation-of-state (EOS)

$$\frac{V(T,P)}{V_0(T)} = 1 - C\ln\left(1 + \frac{P}{B(T)}\right) \tag{1}$$

The parameter B is a function of temperature and depends on the specific system. The parameter C has a universal value of 0.08936 for most of the liquid hydrocarbons including normal paraffins, cycloparaffins, aromatics and fused ring compounds and it is independent of structure or temperature [19]. The isothermal PV data from simulations were also fit with Sun EOS [20]

$$P(T,V) = \frac{B_0(T)}{(n-m)}\left[\left(\frac{V_0(T)}{V}\right)^{n+1} - \left(\frac{V_0(T)}{V}\right)^{m+1}\right] \tag{2}$$

The Sun EOS describes the isothermal compression behavior of polymers in glassy and the melt states except near the glass transition temperature. The generic parameters $n = 6.14$ and $m = 1.16$ for polymer systems were utilized. The parameter B_0 represents the isothermal bulk modulus at zero pressure [25].

B. Calculation of bulk-modulus as a function of temperature and pressure from EOS

The isothermal bulk modulus is defined as [21]

$$\kappa_T(T,P) = -V\left(\frac{\partial P}{\partial V}\right)_T \tag{3}$$

For the Tait EOS κ_T is therefore

$$\kappa_T = \left[1 - C\ln\left(1 + \frac{P}{B(T)}\right)\right]\left[\frac{B(T)+P}{C}\right] \tag{4}$$

which at zero pressure reduces to

$$\kappa_T = \frac{B(T)}{C} \tag{5}$$

In order to find the bulk modulus as a function of temperature using the Tait EOS, an exponential temperature dependence of parameter B was assumed [22]

$$B(T) = B_1 \exp(-B_2 T) \tag{6}$$

The values of $B(T)$, obtained from the fit of the Tait EOS at two temperatures (600 K and 700 K) were used to calculate the parameters B_1 and B_2, thereby allowing us to extrapolate the bulk modulus to lower temperatures.

The Sun EOS yields an isothermal bulk modulus [25]

$$\kappa_T = \frac{B_o(T)}{(n-m)}\left\{(n+1)\left[\frac{V_o(T)}{V(T,P)}\right]^{n+1} - (m+1)\left[\frac{V_o(T)}{V(T,P)}\right]^{m+1}\right\} \tag{7}$$

Where subscript "$_O$" denotes the zero pressure values. The parameters n and m are independent of pressure and temperature.

C. Calculation of thermodynamic and transport properties from MD simulation trajectories

The κ_T corresponding to a given temperature and pressure can be calculated from volume fluctuations in NPT simulation by [23]

$$\kappa_T = \langle V \rangle K_B T / \left\langle \left(V - < V >\right)^2 \right\rangle_{NPT} \tag{8}$$

Where, K_B is Boltzmann constant, V is the instantaneous volume of the system and $\langle .. \rangle$ represents the ensemble average.

The thermal expansion coefficient α was evaluated using the following relation [26]

$$\alpha = \frac{1}{V}\left(\frac{\partial V}{\partial T}\right)_P \tag{9}$$

The quantity in parenthesis was calculated from the slope of the isobaric volume vs. temperature curves obtained from simulation.

The self-diffusion coefficient for Estane chains in the pure melt and in the model PBX-9501 binder at a given temperature and pressure was calculated from the average mean-squared center-of-mass displacement of the polymer chains [24], or

$$D = \lim_{t\to\infty} \frac{\left\langle \left| x(t) - x(0) \right|^2 \right\rangle}{6t} \tag{10}$$

where the brackets represent an ensemble average.

Finally, the zero-frequency shear viscosities of the model PBX-9501 binder and pure Estane melt were calculated as a function of temperature using the Einstein relation [25]

$$\eta = \lim_{t\to\infty} \eta(t) = \lim_{t\to\infty} \frac{V}{6K_B T t}\left(\left\langle \sum_{\alpha\neq\beta} \left(L_{\alpha\beta}(t) - L_{\alpha\beta}(0) \right)^2 \right\rangle \right) \tag{11}$$

where $L_{\alpha\beta}(t) = \int_0^t \sigma_{\alpha\beta}(t')\,dt'$, t is time, $\sigma_{\alpha\beta}$ is the symmetric stress sensor, and V is the volume of the simulation box. The lengths of simulation trajectories were chosen such that $t_{sim} >> \tau_\eta$, where τ_η is the viscosity relaxation time defined as

$$\eta(\tau_\eta) = (1 - e^{-1})\eta(t_{sim} \to \infty) \tag{12}$$

The shear viscosity was calculated by averaging the apparent viscosity data obtained from Eq. 11 for the specified time interval. The details of the methodology used to estimate the apparent average shear viscosity from MD simulation can be found in our previous work on HMX [26].

D. Calculation of viscoelastic properties from MD simulations

The time dependent shear stress modulus, $G(t)$, of the model PBX-9501 binder mixture can be determined directly on time scales accessible to simulations (tens of nanoseconds and shorter) from the stress autocorrelation function as [27]

$$G(t) = \frac{V}{K_B T}\left\langle \sigma_{xy}(t)\sigma_{xy}(0)\right\rangle \tag{13}$$

In this way the high-frequency behavior (glassy regime) of the polymer can be determined. The details for this methodology can be found in earlier reports on the viscoelastic properties of polybutadiene in the glassy regime [28]. At longer times (or low-frequencies) the influence of entanglements on the modulus must be taken into account. This can be done by combining results of MD simulations for unentangled chains (model PBX-9501 binder) and three different reptation models, the Doi- Edwards (DE) model, modified Doi- Edwards (MDE) model, [29] and Milner-McLeish model (MM) [30], for entangled polymer melts yielding the shear stress modulus $G(t)$ for entangled binder in the plateau and terminal regimes. Details on combining results from MD simulations of unentangled polymers with these three models are provided in our previous study on polybutadiene [26,31]. A summary of all parameters used in calculation of $G(t)$ for model PBX-9501 binder from these three models is given in Table 2. Along with the parameter values, a brief description of the parameter and the corresponding symbol (as given in reference 26) are also listed in this table.

Table 2

Parameters used in prediction of *G(t)* of PBX-9501 binder using combined MD simulation and reptation theory

Symbol	Parameter	473 K, 1 atm	vs. *T*	vs. *P*
	Quantities obtained from simulations of the model (unentangled) binder			
M_0	Molecular weight of Estane (g/mol)	2510	2510	2510
N_0	Number of backbone bonds chain	143	143	143
$\langle R^2 \rangle_0$	Mean-square end-to-end distance Estane (Å^2)	1738	1738[a]	1738[b]
C_∞	Characteristic ratio of Estane	5.5	5.5[a]	5.5[b]
ρ	Density (kg/m^3) of simulated binder	1075	Fig. 5b	EOS
D(T,P)	Diffusion coefficient of Estane (Å^2/ps)	3.9 X 10^{-3}	Fig. 7a	Fig. 7b
τ_R^0	Rouse time for Estane chain (ps)	1.5 X 10^4	$\tau_R^0 \sim T/D(T,P)$	
p	Packing length (Å)	2.2	$p \sim \langle R^2 \rangle_0^{-1} \rho^{-1}$	
a	Tube diameter (Å)	44.4	$a \sim p$	
N_e	Number of monomers between entanglements	162	$N_e \sim p^3 \rho$	
G_N	Plateau modulus (MPa)	1.5	$G_N \sim p^{-3} T$	
	Molecular weight dependent quantities			
M	Molecular weight of entangled Estane (g/mol)			
N	Number of backbone bonds in entangled Estane		$N > N_e$	
τ_R	Rouse time for entangled Estane (ps)		$\tau_R = \tau_R^0 (N/N_0)^2$	

[a]These quantities show relatively weak dependence on temperature, which is assumed to be zero for convenience. [b]These quantities show relatively weak dependence on pressure, which was assumed to be zero for convenience.

IV. Results and Discussion

A. Thermodynamic properties

PV isotherms for the model PBX-9501 binder at 600 K and 700 K are shown in Fig. 2(a) and Fig. 2(b) respectively. Also shown are fits of the Tait and Sun EOS to the simulation data. The parameters obtained in fitting the Tait and Sun EOS to the PV data from MD simulations are listed in Table 3. Both EOS represent the PV data accurately over the range of pressures investigated.

Table 3

Parameters obtained from fitting simulation data to different empirical EOS

	Parameter B[a]	
	600 K	700 K
EOS		
Tait	680 atm	396 atm
Sun	8516 atm	5050 atm

[a]For the Tait EOS parameter B is same as in Eq. 1. For the Sun EOS this represents the value of B_0 in Eq. 2.

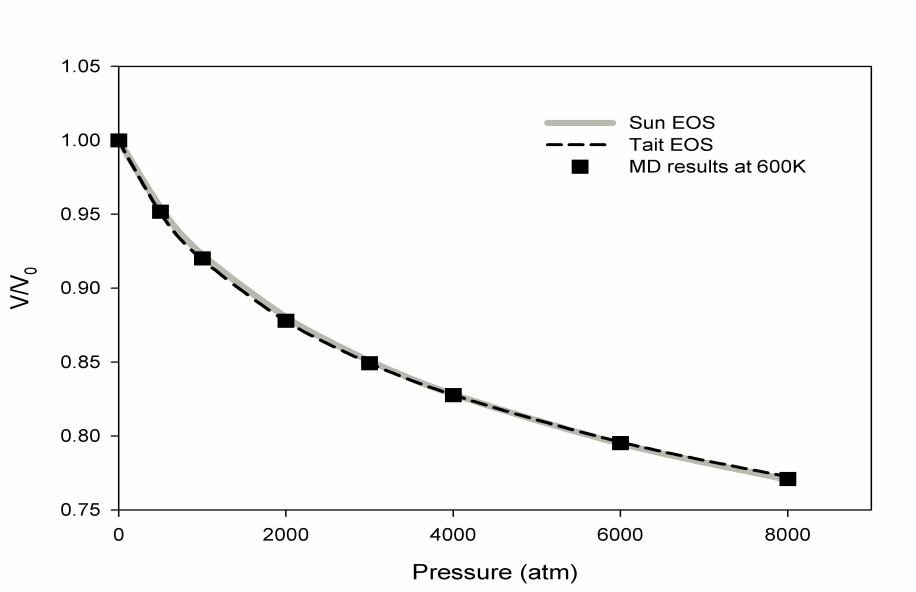

Figure 2(a)

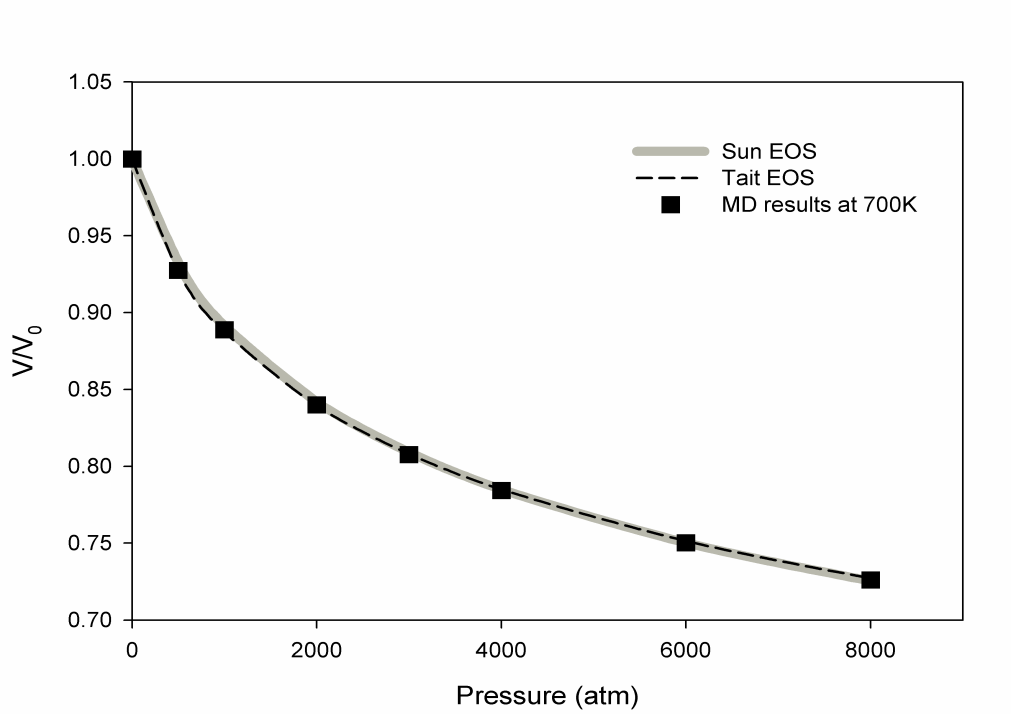

Figure 2(b)

Figure 2. Volume as a function of pressure for model PBX-9501 binder for the (a) 600 K and (b) 700 K isotherms. Error bars for MD data, estimated using the standard error calculation (90% confidence limits), are smaller than the symbols.

The pressure dependent bulk moduli for the model PBX-9501 binder calculated using Eq. 8 are shown in Fig. 3(a) at 600 K and Fig. 3(b) at 700 K. An increase in pressure from 1 atm to 8000 atm results in a significant increase in the bulk modulus of the model PBX-9501 binder. Also shown in Fig. 3 is the bulk modulus obtained from the Tait (Eq. 5) and Sun (Eq. 7) EOS. Excellent agreement between bulk moduli obtained from both EOS and MD at both temperatures can be seen.

In Fig. 4, the bulk modulus obtained from MD simulations of binder at 1 atm is shown as a function of temperature. As expected, the bulk modulus decreases with increasing temperature.

The temperature dependent bulk modulus obtained for binder from the Tait EOS is also shown in Fig. 4. A good agreement between the EOS and fluctuation-based MD values for the bulk modulus can be seen. The bulk modulus for binder obtained from the extrapolated Tait EOS (3.9 GPa) and directly from MD simulations (3.8 GPa) at 298 K are in good agreement with the experimental value of 3.6 GPa reported by Clements *et al.* [32].

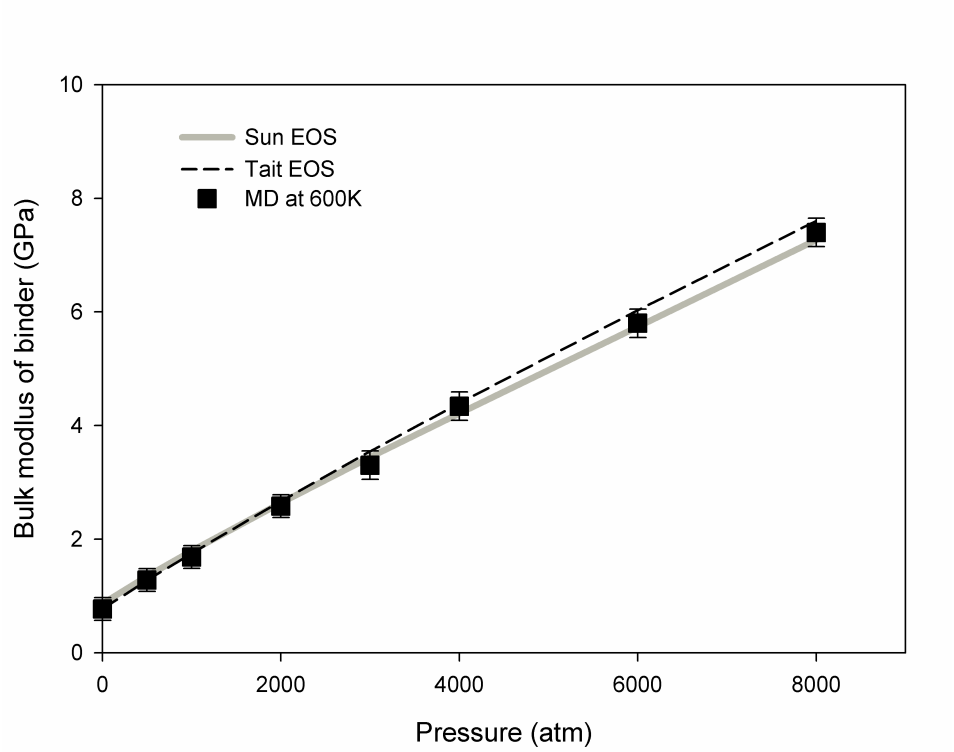

Figure 3(a)

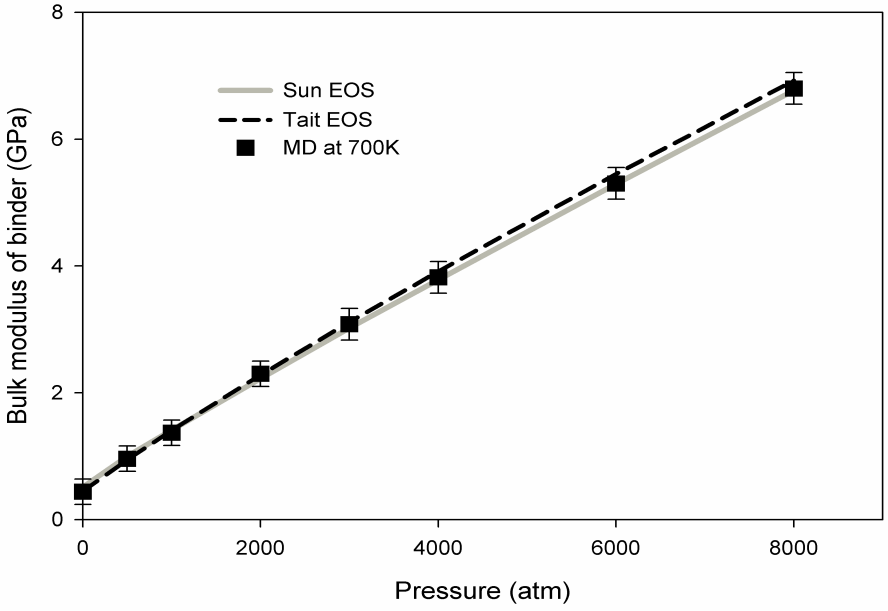

Figure 3(b)

Figure 3. Bulk modulus for model PBX-9501 binder a function of pressure for the (a) 600 K and (b) 700 K isotherms. Error bars for MD data were estimated using the standard error calculation (90% confidence limits).

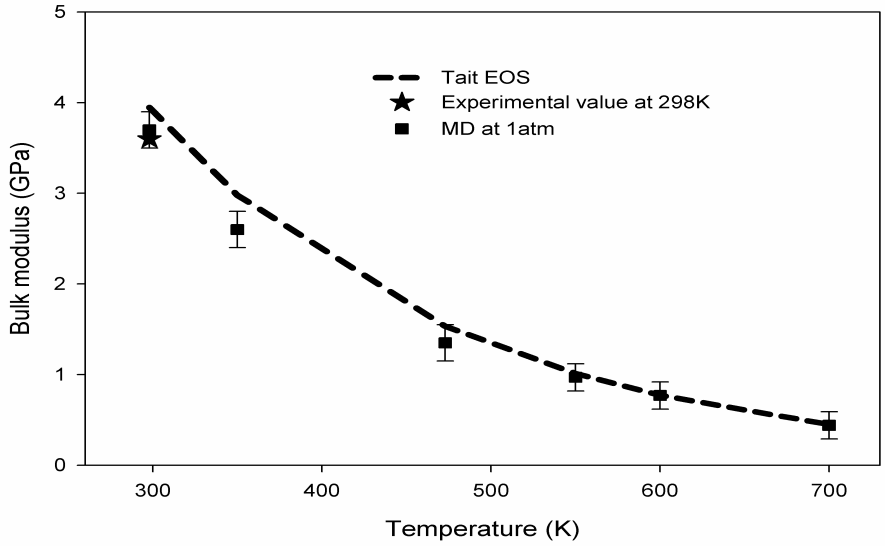

Figure 4. Bulk modulus of model PBX-9501 binder as a function of temperature at 1atm. Error bars for MD data were estimated using the standard error calculation (90% confidence limits).

Finally, Fig. 5(a) and Fig. 5(b) show the temperature dependent density and thermal expansion coefficients obtained from MD simulations at 1 atm pressure for the pure Estane melt and model PBX-9501 binder. Fig. 5a reveals that the binder mixture is denser than pure Estane, consistent with the fact that the nitroplasticizer is significantly denser (1.383-1.397 g/cm^3 at 298 K [25]) than Estane. Interestingly, Fig. 5(b) reveals that the thermal expansion coefficient of the relatively dense model PBX-9501 binder is about 15-20% greater than that of the pure Estane melt over the temperature range investigated.

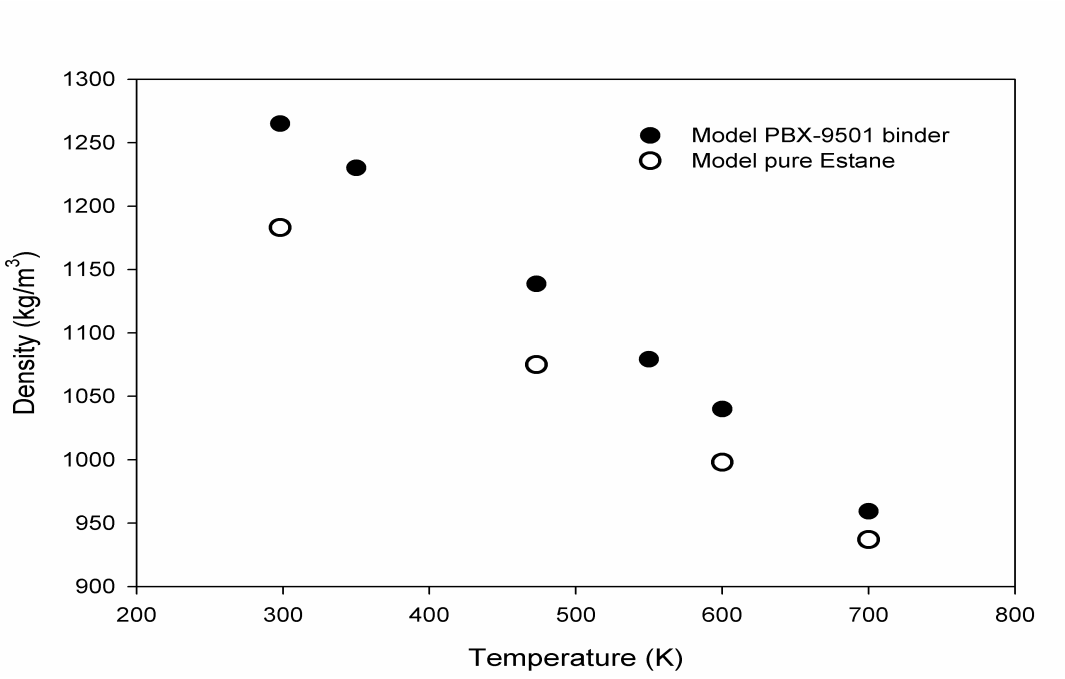

Figure 5(a)

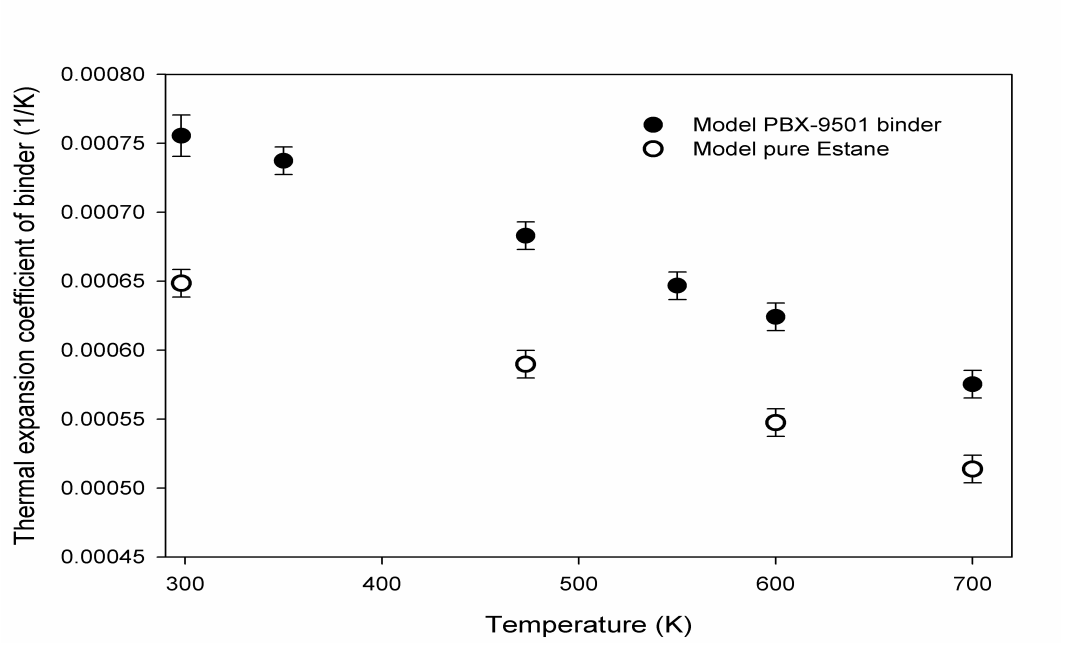

Figure 5(b)

Figure 5. (a) Density as a function of temperature for model PBX-9501 binder and pure Estane. (b) Thermal expansion coefficient for model PBX-9501 binder and pure Estane. Error bars were estimated using the standard error calculation (90% confidence limits).

B. Viscosity and Self-Diffusion of Estane

The viscosity of the pure Estane melt and model PBX-9501 binder is shown as a function of inverse temperature in Fig. 6. The addition of plasticizer reduces the viscosity of Estane as well the temperature dependence of the viscosity. The viscosity data for pure estane and binder were fit assuming an Arrhenius temperature dependence,

$$\ln(\eta) = A + \frac{B}{T} \tag{14}$$

with $A = -3.0, B = 2460$ for model PBX-9501 binder and $A = -3.9, B = 3490$ for pure Estane melt.

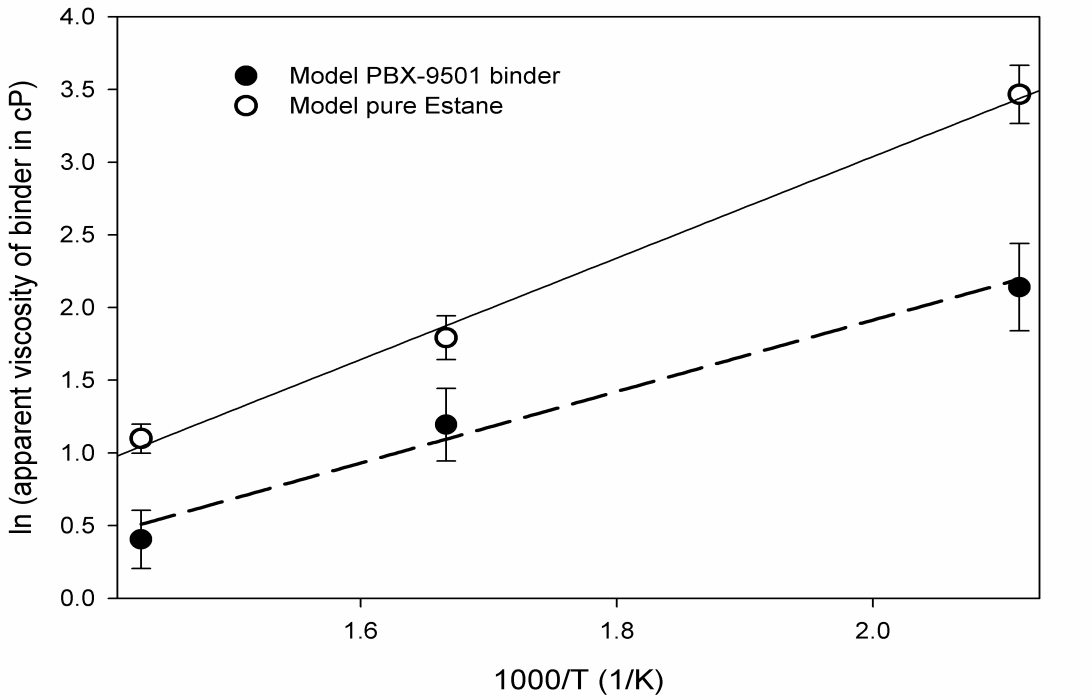

Figure 6. Apparent viscosity of the model PBX-9501 binder and pure Estane as a function of inverse temperature. Error bars were estimated using the standard error calculation (90% confidence limits). Arrhenius fits are shown.

The self-diffusion coefficient of the Estane chains in the model PBX-9501 binder and pure melt is shown as a function of inverse temperature in Fig. 7(a). The self-diffusion of Estane is faster in binder than in pure melt at all temperatures investigated. The temperature dependence of the self-diffusion coefficient for Estane chains in the pure melt and model PBX-9501 obtained using the Stokes-Einstein relation and an Arrhenius temperature dependence for the viscosity,

$$D(T) \propto \frac{T}{\eta} \Rightarrow \ln[D(T)] = C + \ln(T) - \frac{B}{T} \tag{15}$$

is also shown in Fig. 7a. Here, values of $C = -35.2, B = 1920$ for binder and $C = -33.7, B = 3396$ for Estane were obtained. The activation energy, ΔE_{diff}, can be obtained by multiplying B with universal gas constant in appropriate units. The effect of pressure on the diffusion of Estane in binder at 600 K and 700 K is shown in Fig. 7(b). Increasing the pressure from 1 atm to 8000 atm reduces the diffusion coefficient by almost two orders of magnitude.

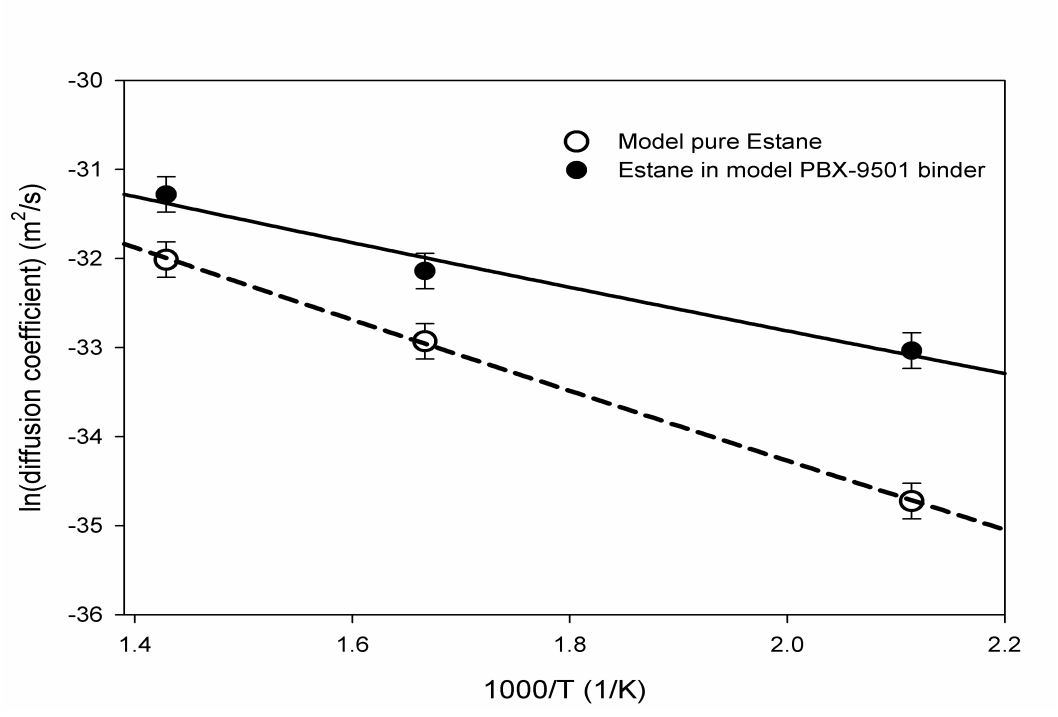

Figure 7(a)

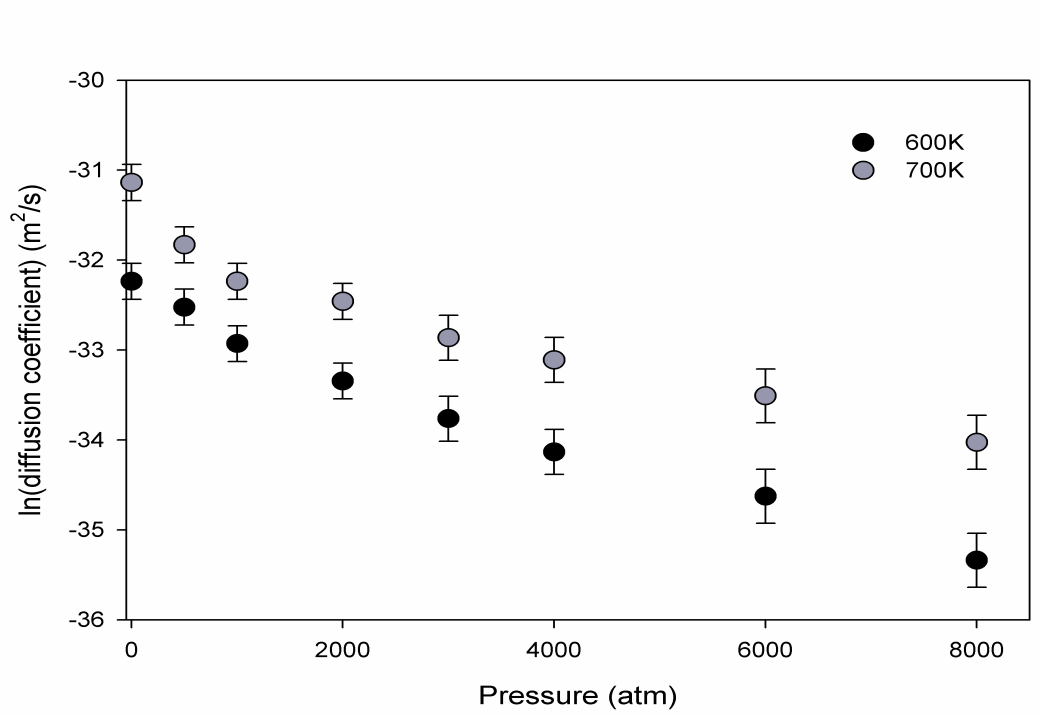

Figure 7(b)

Figure 7. (a) Self diffusion coefficient of Estane in the model PBX-9501 binder model pure Estane as a function of inverse temperature. The fits using Eq. 14 are represented by a solid line for model PBX-9501 binder and dashed line for model pure Estane. (b) Self diffusion coefficient of Estane in model PBX-9501 binder as a function of pressure at two temperatures. Error bars were estimated using the standard error calculation (90% confidence limits).

C. Viscoelastic Properties at 473 K

The shear stress relaxation modulus for model PBX-9501 binder at 473 K is shown in Fig. 8(a). Predictions for a highly entangled polymer (85 KDa) are shown. The modulus for times shorter than the plateau regime was obtained directly from the stress tensor ACF (Eq. 13) from a 60 ns MD simulation of the model PBX-9501 binder (unentangled Estane chains) at 473 K. The shear stress relaxation modulus of binder in the plateau and terminal regimes was calculated by combining MD simulation with the three reptation models discussed above (see also Table 2).

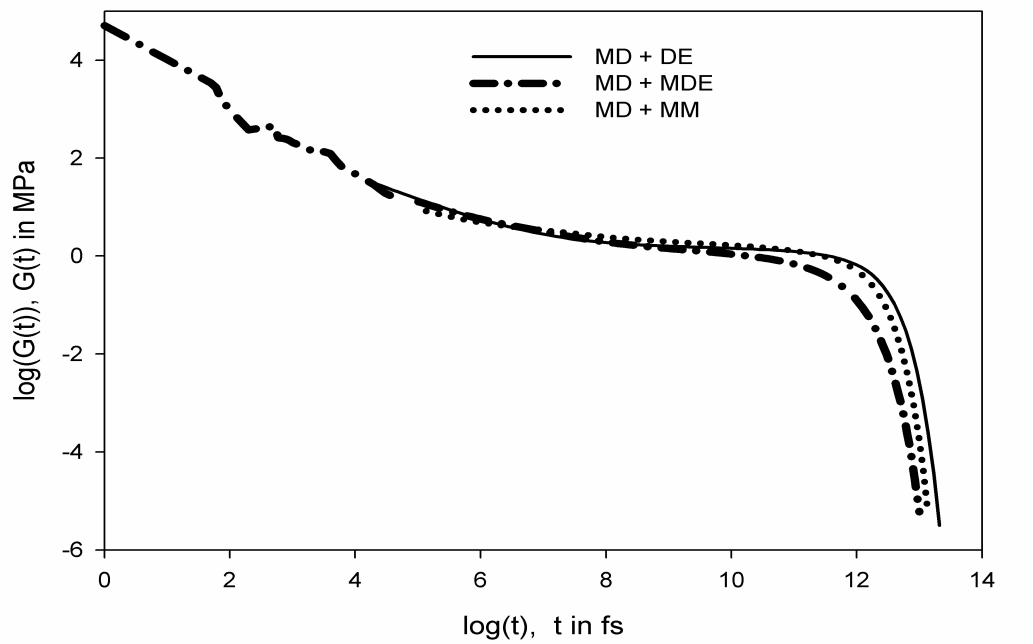

Figure 8(a)

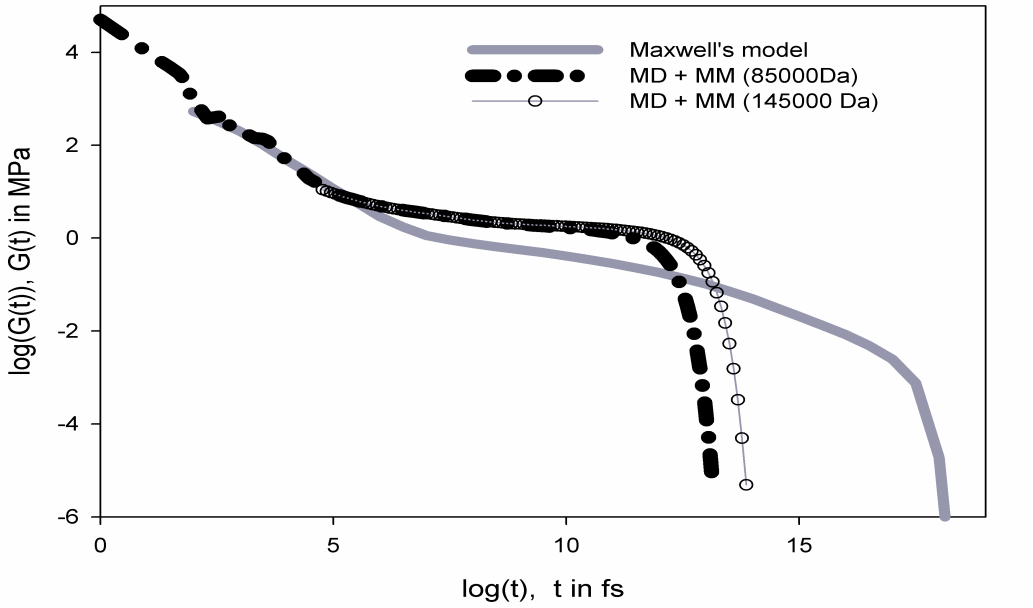

Figure 8(b)

Figure 8: (a) G(t) for PBX-9501 binder (85 KDa Estane) from three different models: Doi-Edwards (DE), Modified Doi-Edwards (MDE) and and Milner-McLeish (MM) model. (b) Comparison of G(t) for PBX-9501 binder obtained from combination of the MM model and MD data with the Maxwell model for binder with Estane 5703.

All three reptation models yield similar results for the plateau modulus and terminal relaxation time. In Fig. 8(b) predictions of *G(t)* using the Milner-McLeish (MM) model are compared with the Maxwell model developed for *G(t)* of PBX-9501 binder based on experimental measurements over a temperature range of -150ºC (123 K) to 75ºC (348 K) [33]. The time-temperature shift factor obtained from the Maxwell model for PBX-9501 was used to shift *G(t)* to 473 K for comparison with simulation predictions.

The short-time response (glassy and Rouse regimes) obtained from simulation are in good agreement with extrapolation (to 473 K) of the Maxwell viscoelastic model. However, differences between $G(t)$ obtained from extrapolation of the Maxwell model fitted to experimental data and the prediction from reptation theory can be observed for the plateau and the terminal zone. Particularly, Estane-5703, utilized in the experimental binder, appears to exhibit a much longer terminal relaxation time than predicted by reptation theory. As seen from Fig. 8(b), increasing the molecular weight of Estane chains from 85 KDa to 145 KDa, the highest molecular weight observed in experiments, does not increase the terminal relaxation time predicted from the MM reptation model enough to account for the differences with the extrapolation of the Maxwell model.

The plasticized (50 wt% nitroplasticizer) Estane (Estane 5703) exhibits a hard segment T_g of abount 72 ºC and a soft segment T_g of about -45 ºC [34]. Thermodynamic incompatibility between hard and soft segments results in microphase separation of hard segments into hard domains. At temperatures somewhat above 72ºC the hard domains are completely disrupted [35]. The Maxwell model discussed above is based on experiment measurements for temperatures below the order-disorder temperature (ODT) wherein it is to be expected that hard domains can act as physical crosslinks, dramatically increasing the terminal relaxation time compared to that

predicted by reptation theory, consistent with the behaivor observed in Fig. 8(b). We believe that the Maxwell model yields a superior estimate of $G(t)$ for the Estane 5703-based binder at temperatures below the ODT than provided by our combined simulation and reptation theory predictions. However, Fig. 8(b) reveals that the Maxwell model should not be extrapolated to temperatures above the ODT. Here, we believe that reptation theory should provide a good estimate of $G(t)$.

Our simulations not only allow for estimate of $G(t)$ for PBX-9501 binder at 473 K and 1 atm (for any Estane molecular weight), as illustrated in Fig. 8, but can also be utilized to estimate $G(t)$ as a function of temperature and pressure in the plateau and terminal regimes for temperatures above the ODT of Estane. Specifically, the temperature dependence of the binder density (Fig. 5a) and of the self-diffusion coefficient of Estane in binder (Fig. 6) can be utilized in the combined MD simulation/reptation approached presented in this work to predict *G(t)* of PBX-9501 binder at 1 atm for any molecular weight of Estane at temperatures above the ODT (see Table 2 for the estimation of temperature-dependent model parameters). Similarly, an EOS (Table 2), utilized to obtain the pressure-dependent density, combined with the pressure dependent self-diffusion coefficient (Fig. 7b), can be employed to estimate the influence of pressure on *G(t)* of PBX-9501 binder over a wide range of pressures for any molecular weight of Estane, again at temperatures above the ODT (see Table 2 for the estimation of pressure-dependent model parameters). The temperature (Fig. 6) and pressure dependence of the viscosity of the model PBX-9501 binder would in principle provide an even better estimate of the the temperature and pressure dependence of *G(t)*. Unfortunately, we have found that obtaining good estimates of the viscosity of the model binder at high pressure is difficulty due to slow dynamics.

[1][] Espada, L. I., Mang, J. T., Orler, B., Wrobleski, D. A., Langlois, D. A., Hjelm, R. P. 2001. *Polymer Preprints*. 42(2): 693.

[2][] Asay, B. W., Henson, B. F., Smilowitz, L., Dickson, P. M., 2003. *J. Energ. Mater.* 21:223-235.

[3][] Parker, G. R., Peterson, P. D., Asay, B. W., Dickson, P. M., Perry, W. L., Henson, B. F., Smilowitz, L., Oldenborg, M. R. 2004. *Propellants, Explos., Pyro.* 29(5):274-281.

[4][] Swallowe, G.M., Field, J.E. 1982. *Proc. R. Soc. London, Ser. A.* 379:389

[5][] Kipp, M.E., Nunziato, J.W., Setchell, R.E., Walsh, E.K. *Proceedings of the Seventh Symposium (International) on Detonation.* 1989.

[6][] Moonan, W.K., Tschoegl, N.W. 1985. *J. Polym. Sci.* 23(4):623.

[7][] Losi, G. U., Knauss, W.G. 1992. *Polym. Sci. Eng.* 32(8):542-557.

[8][] Knauss, W.G., Sundaram, S. 2004. *J. Appl. Phys.* 96(12):7254-7266.

[9][] Smith, G. D., Bedrov, D., Byutner, O. G., Borodin, O., Ayyagari, C. and Sewell, T. D. 2003. *J. Phys. Chem. A.* 107:7552.

[10][] Davande, H., Borodin, O., Smith, G.D., Sewell, T.D. 2005. *J. Energ. Mat.* 23(4):205-37.

[11][] http://lucretius.mse.utah.edu/

[12][] Nosé, S., 1984. *J. Chem. Phys.*, 81:511-519

[13][] Hoover, W. G., 1985. *Phys. Rev. A*, 31:1695-1697

[14][] Anderson, H. C., 1980. *J. Chem. Phys.*, 72:2384-2393

[15][] Ryckaert, J., Ciccotti, G., Berendsen, H. J. C. 1977. *J. Comput. Phys*. 23: 327

[16][] Darden, T., York, D. and Pedersen, L. 1993. *J. Chem. Phys.* 98:10089

[17][] Martyna, G. J., Tuckerman, M. E., Tobias, D. J. and Klein, M. L. 1996. *Molecular physics.* 87(5): 1117

[18][] Nanda, V.S., Simha, R. 1964. *J. Chem. Phys.* 41:1884-85.

[19][] Cutler, W.G., McMickle, R.H., Webb, W., Schiessler, R.W. 1958. *J. Chem. Phys.* 29(4):727-740.

[20][] Sun, Z., Song, M., Yan, Z. 1992. *Polymer.* 33:328-331.

[21][] Smith, J. M., Van Ness, H. C., Abbott, M. M. 2001. Introduction to chemical engineering thermodynamics. Sixth Edition. McGraw-Hill Companies Inc. New York.

[22][] Sachdev, V.K., Yahsi, U., Jain, R.K. 1998. *J. Polym. Sci. Part B. Polym. Phys.* 36:841-850.

[23][] Allen, M. P., Tildesley, T. J. 1987. Computer Simulations of Liquids. Oxford University Press Oxford. U.K.

[24][] Frenkel, D., and Smit, B. 2002. Understanding molecular simulations. From algorithms to applications. Second Ed. Academic Press. San Diego. California. USA.

[25][] Haile, J.M. 1992. Molecular Dynamics Simulations. Wiley. New York.

[26][] Bedrov, D., Smith, G. D., Sewell, T. D. 2000. *J.Chem.Phys.* 112. 7203.

[27][] Doi, M., and Edwards, S. F. 1986. The theory of polymer dynamics. Oxford Science Publications. New York. USA.

[28][] Byutner, O., Smith, G.D., 2002. *Macromolecules.* 35. 3769-3771

[29][] Doi, M. 1981. *J. Polym. Sci. Polym. Lett.* 19. 265.

[30][] Milner, S. T. and McLesih, T. C. B. 1998. *Phys. Rev. Lett.* 81. 725-728.

[31][] Byutner, O., Smith, G.D., 2001. *Macromolecules.* 34. 134-139

[32][] Clements, B.E., Mas, E.M. 2004. *Modelling Simul. Mater. Sci. and Eng.* 12:407-421.

[33][] Mas, E.M.; Clements, B.E. 2002. *Shock Compression of Condensed Matter.* 661.

[34][] Hoffman, D.M., 2002. *J. Appl. Polym. Sci.* 83. 1009-1024.

[35][] Hawley, M.E., Orler, E.B., Wrobleski, D.A., Hjlem, R.P., Brown, G.W. 2001. *Mat. Res. Soc. Symp. Proc.* 661. KK4.7.1-KK4.7.6.